Available online at www.sciencedirect.com

SCIENCE DIRECT®

Tectonophysics 406 (2005) 115–139

TECTONOPHYSICS

www.elsevier.com/locate/tecto

Upper mantle structure of the South American continent and neighboring oceans from surface wave tomography

Maggy Heintz [a,b,*], Eric Debayle [c], Alain Vauchez [a]

[a] *Laboratoire de Tectonophysique, Université Montpellier II, 1 Place Eugène Bataillon, Case courrier 049, 34095 Montpellier, France*
[b] *Research School of Earth Sciences, Australian National University, Mills Road, Canberra, Australia*
[c] *Institut de Physique du Globe, Ecole et Observatoire des Sciences de la Terre, CNRS and Université Louis Pasteur, Strasbourg, France*

Received 28 June 2004; received in revised form 29 April 2005; accepted 9 May 2005
Available online 25 July 2005

Abstract

We present a new three-dimensional SV-wave velocity model for the upper mantle beneath South America and the surrounding oceans, built from the waveform inversion of 5850 Rayleigh wave seismograms. The dense path coverage and the use of higher modes to supplement the fundamental mode of surface waves allow us to constrain seismic heterogeneities with horizontal wavelengths of a few hundred kilometres in the uppermost 400 km of the mantle.

The large scale features of our tomographic model confirm previous results from global and regional tomographic studies (e.g. the depth extent of the high velocity cratonic roots down to about 200–250 km).

Several new features are highlighted in our model. Down to 100 km depth, the high velocity lid beneath the Amazonian craton is separated in two parts associated with the Guyana and Guapore shields, suggesting that the rifting episode responsible for the formation of the Amazon basin has involved a significant part of the lithosphere. Along the Andean subduction belt, the structure of the high velocity anomaly associated with the sudbduction of the Nazca plate beneath the South American plate reflects the along-strike variation in dip of the subducting plate. Slow velocities are observed down to about 100 km and 150 km at the intersection of the Carnegie and Chile ridges with the continent and are likely to represent the thermal anomalies associated with the subducted ridges. These lowered velocities might correspond to zones of weakness in the subducted plate and may have led to the formation of "slab windows" developed through unzipping of the subducted ridges; these windows might accommodate a transfer of asthenospheric mantle from the Pacific to the Atlantic ocean. From 150 to 250 km depth, the subducting Nazca plate is associated with high seismic velocities between 5°S and 37°S. We find high seismic velocities beneath the Paraná basin down to about 200 km depth, underlain by a low velocity anomaly in the depth range 200–400 km located beneath the Ponta Grossa arc at the southern tip of the basin. This high velocity anomaly is located southward of a narrow S-wave low velocity structure observed between 200 and 500–600 km depth in body wave studies, but irresolvable with our long period datasets. Both

* Corresponding author. Research School of Earth Sciences, Australian National University, Mills Road, Canberra, Australia. Tel.: +61 2 6125 0339; fax: +61 2 6257 2737.
E-mail addresses: maggy@rses.anu.edu.au (M. Heintz), Eric.Debayle@eost.u-strasbg.fr (E. Debayle), vauchez@dstu.univ-montp2.fr (A. Vauchez).

0040-1951/$ - see front matter
doi:10.1016/j.tecto.2005.05.006

anomalies point to a model in which several, possibly diachronous, plumes have risen to the surface to generate the Paraná large igneous province (LIP).

Keywords: Upper mantle; Tomography; Surface wave higher modes; South American continent; Cratonic roots; Subduction

1. Introduction

The South American continent is the end product of a complex evolution of the continental lithosphere that began in Archean times and has involved successive periods of gathering and dispersion of continental landmasses, which are expected to have left a lasting imprint on the lithospheric mantle. Several major geological units have been progressively accreted to Archean nuclei (Fig. 1). Archean protolith-ages found in younger mobile belts strongly suggest that the Archean component was originally significantly larger than observed today (Cordani and Brito Neves, 1982). The largest and best preserved Archean terranes are exposed in the Amazonian and São Francisco cratons (Teixeira et al., 2000). The Amazonian craton, one of the largest cratonic provinces in the world, involves two main blocks, the Guyana and the Guapore shields, located to the north and south of the Amazon basin. Both shields include terranes of the same age and nature, and probably formed a single craton before the Amazonian rifting episode (Cordani and Brito Neves, 1982; Tassinari et al., 2000). The São Francisco craton is located in southeast Brazil and involves an Archean nuclei surrounded by Paleoproterozoic terranes (Teixeira et al., 2000).

The gathering of the South American cratons and their African counterparts (West-African, Congo and Kalahari cratons) during the Neoproterozoic led to the formation of the Gondwana supercontinent. The collision of the pre-existing cratons resulted from the closure of several oceanic basins and led to the formation of continental-scale orogenic belts that wrap around the cratonic domains.

Several diachronous flexural basins formed on the western Gondwana at the end of and after the Neoproterozoic orogeny. Marine and continental sedimentary deposits are particularly well represented in five large (500,000 to 1,000,000 km^2) basins (Milani and Thomaz Filho, 2000): the Amazonian and Solimões rifts that crosscut the Amazonian craton, the Parnaiba (NE-Brazil), the Chaco (S Brazil) and the Paraná (N-Argentina) flexural basins (Fig. 1). The Paraná basin was filled with flood basalts between 137 and 127 Ma and represents one of the main Large Igneous Province (LIP) in the world. Together with its African counterpart, the Etendeka LIP, it has been associated with the surface expression of the Tristan da Cunha mantle plume (Turner et al., 1994). Regional surface wave studies show high S-wave velocity compatible with cratonic lithosphere down to about 200 km beneath the Paraná basin (Snoke and James, 1997). At greater depths, an unexpected vertical cylindrical low velocity anomaly has been found between 200 and 500–600 km from teleseismic P- and S-wave tomography (VanDecar et al., 1995; Schimmel et al., 2003). This cylindrical low velocity anomaly has been interpreted as the fossil conduit of the Tristan da Cunha plume responsible for the Paraná flood basalts (VanDecar et al., 1995; Schimmel et al., 2003).

The Andean Cordillera subduction belt bounds the western margin of the continent over 8000 km long (e.g., Ramos and Aleman, 2000) and results from the subduction of the Nazca plate beneath South America. The subducting Nazca plate is generally associated with high seismic velocities in tomographic studies (e.g., Engdahl et al., 1995; James and Snoke, 1990; Schneider and Sacks, 1987; Wortel, 1984) but the depth extent of the anomaly and the continuity of the slab at depth is still debated. The geometry of the slab is characterized by two main features: (1) a gap of seismicity between 300 and 500 km highlighted by the distribution of hypocentres along the subduction plane (Fig. 2b) and (2) along-strike variations in dip from subhorizontal flat-slab segments to normal subduction (Barazangi and Isacks, 1979; Cahill and Isacks, 1992; Engdahl et al., 1998). Between 2°S and 15°S and between 28°S and 33°S, the subduction is "flat" (subhorizontal), whereas elsewhere, it is "normal" (Andean type), dipping around 30° (Fig. 2a). Regions above "flat" subduction segments are characterized by a lack of volcanic activity since the late Miocene, whereas

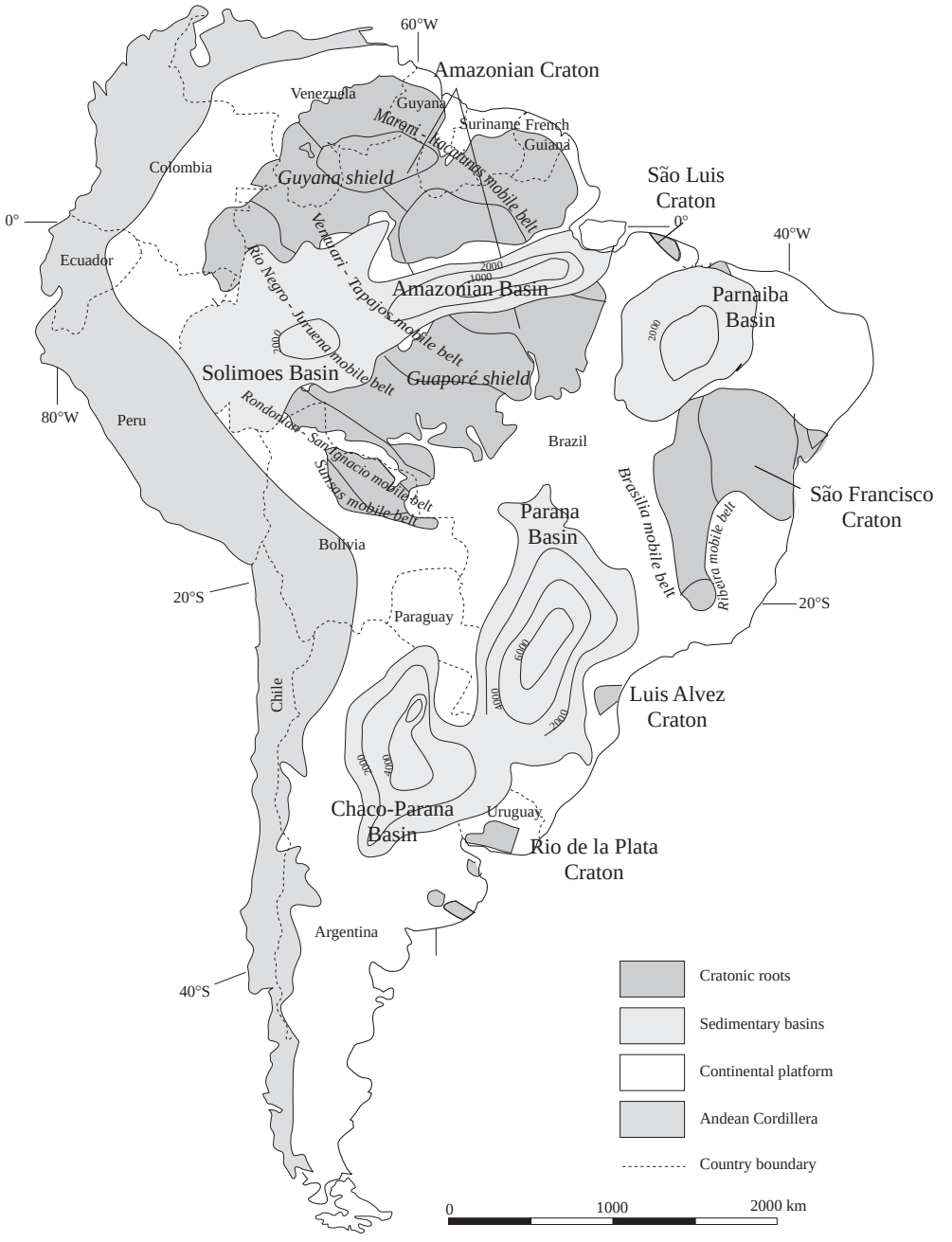

Fig. 1. Geotectonic map of South America (adapted from Cordani et al., 2000, for the location of the cratonic domains, and from Milani and Thomaz Filho, 2000, for the location of the sedimentary basins).

those above a "normal" dipping subduction segment are volcanically active (Fig. 2a). The Central Volcanic Zone (CVZ) corresponding to the Altiplano-Puna plateau (Allmendinger et al., 1997) is of particular interest, since it is characterized by an exceptionally thick crust (70–80 km) associated with abundant volcanism. Several local body wave studies have been performed in the Andes at ca. 20°S latitude, to

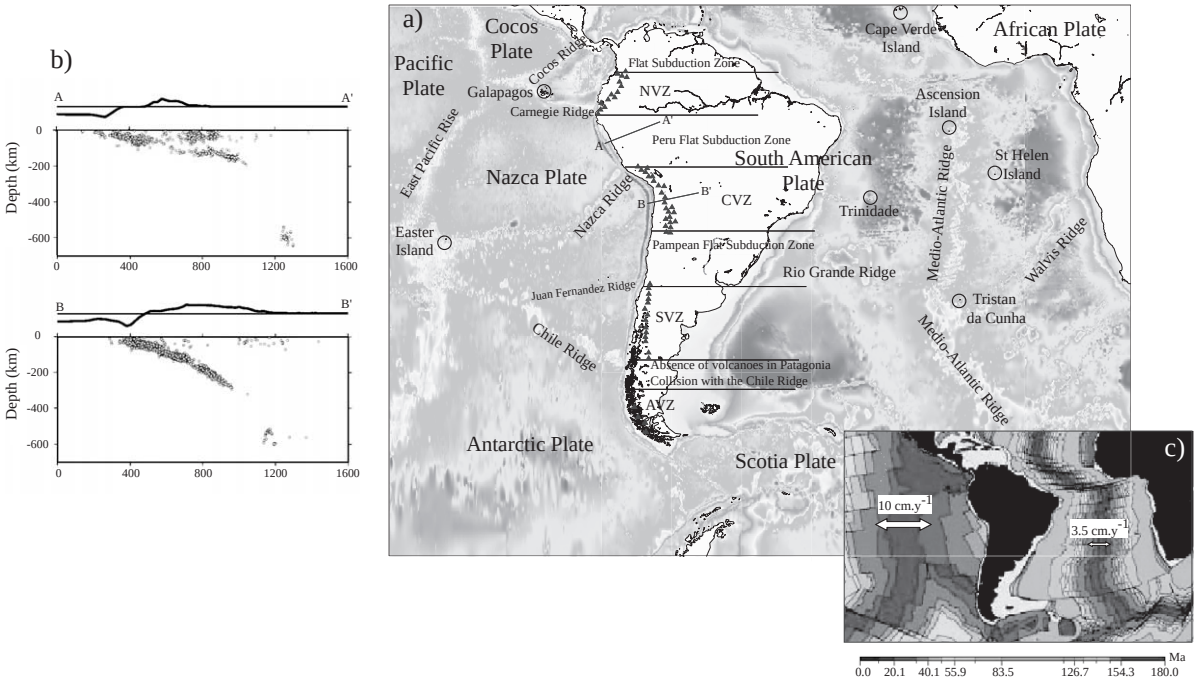

Fig. 2. (a) Bathymetric map of the Pacific and Atlantic oceans surrounding the South American plate. The names of the main ridges together with the different hotspots are shown. On the South American continent, the along-strike variations in the dip of the Nazca plate subducting beneath the South American plate are symbolized either by 'flat subduction zones' or NVZ (Northern Volcanic Zone), CVZ (Central Volcanic Zone), SVZ (Southern Volcanic Zone) and AVZ (Austral Volcanic Zone). Black triangles symbolize volcanoes. (b) Representation of the seismicity with respect to depth for the cross-sections (AA′ and BB′) shown on map (a). (c) Map of isochrons for both the Pacific and Atlantic ocean floors.

investigate the processes leading to this huge crustal thickening. P and S-wave local tomographic studies (Dorbath and Masson, 2000; Masson et al., 2000) as well as attenuation tomographic models (Haberland and Rietbrock, 2001; Myers et al., 1998; Schurr, 2001) show low seismic velocities and large attenuation below the Altiplano-Puna near about 20°S and down to approximately 100 km depth. From theses observations, it was suggested that: (1) fluids released from the subducting lithosphere triggered partial melting of the mantle wedge and the lower–middle crust, and (2) crustal thickening is increased by underplating of magmas generated by partial melting of the mantle wedge. This latter hypothesis is however not uniformly accepted, and Swenson et al. (2000), for instance, suggested from broadband regional waveform modelling that the crustal thickening might be predominantly caused by tectonic shortening of felsic crust, rather than by underplating or magmatic intrusion from the mantle.

At the continental scale, global upper mantle S-wave tomographic models generally display high velocity anomalies extending down to 250–300 km beneath the cratons of South America (Grand, 1994; Mégnin and Romanowicz, 2000; Trampert and Woodhouse, 1995) although a recent high resolution global surface wave model favors a shallower high velocity lid (Ritsema et al., 2004).

Vdovin et al. (1999) produced regional fundamental mode surface wave group velocity maps of South America at periods between 30 and 150 s. These tomographic maps result from the inversion of several thousand average group velocity measurements for surface wave paths and provide at each geographical point a weighted average of the S-wave structure over a depth interval that depends on the period, allowing only a rough estimation of the depth location of seismic heterogeneities in the uppermost 200–250 km of the mantle. In the resulting group velocity maps nevertheless, the sedimentary basins are seen at 30 s period, the

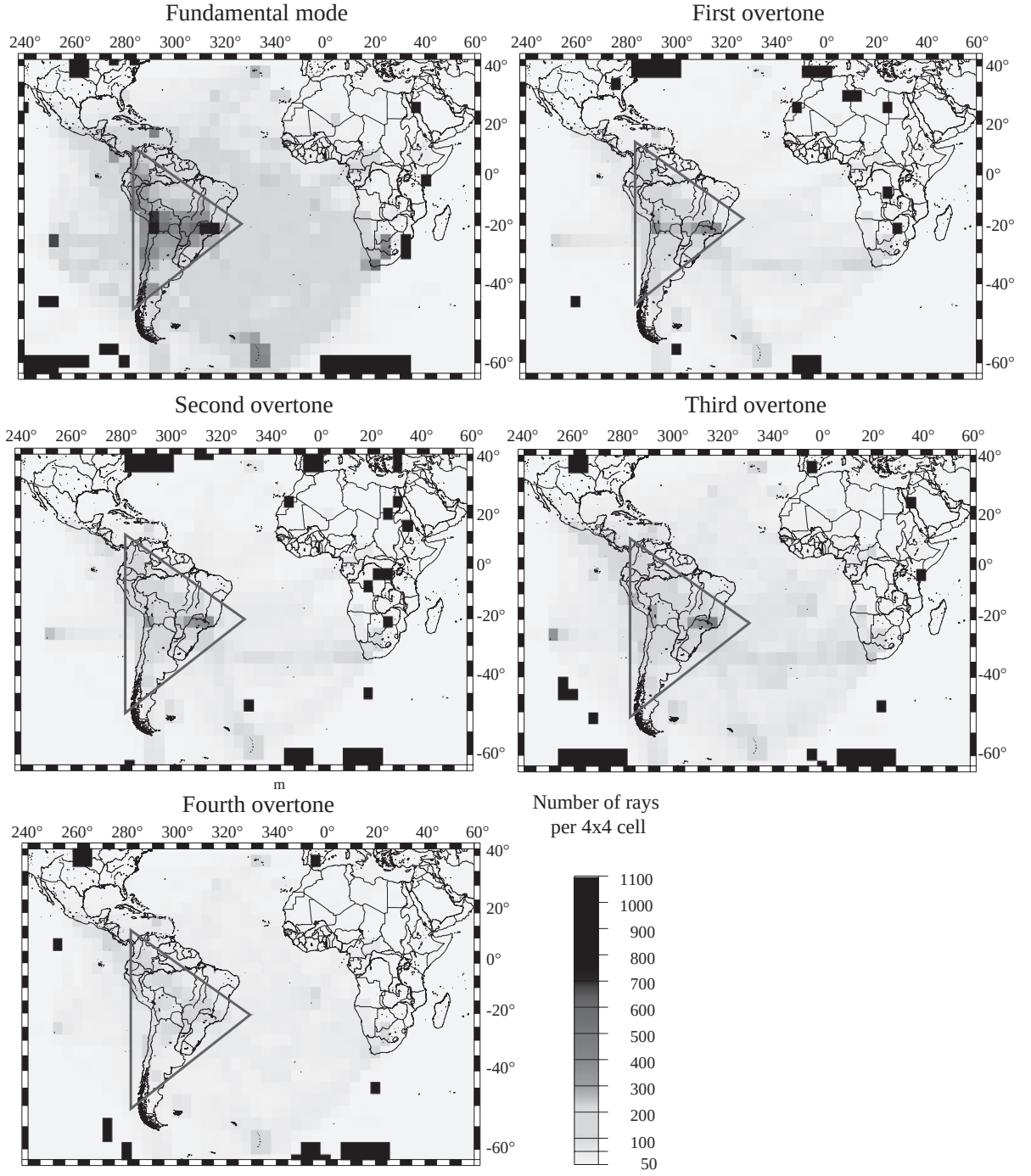

Fig. 3. Ray density maps for $4^\circ \times 4^\circ$ cells, for the fundamental mode and the four overtones. The black triangle symbolizes the region with the highest ray density.

variations of crustal thickness at 50 s period and the depth extent of continental cratonic roots at 100 s period. In this model, a single, high velocity anomaly is also observed beneath the Amazonian and São Francisco cratons down to approximately 200 km depth.

Fundamental mode dispersion curves have been inverted by Silveira and Stutzmann (2002) to build a 3D S-wave velocity model of the South Atlantic ocean and neighboring continents. This model covers South America with only a limited number of paths and provides poor resolution below 250 km depth; it however shows a large domain of high seismic velocities that includes both the Amazonian and São Francisco cratons and is imaged at depth down to 300 km. Van der Lee et al. (2001, 2002) inverted both fundamental and higher modes of Rayleigh waves to improve resolution deeper than 250 km but their restricted data set of about 500 surface waveforms has an extremely heterogeneous coverage and provides good horizontal resolution only beneath limited parts of the continent. In their model, however, the upper mantle structure is well resolved beneath the western Amazonian craton and displays a high velocity anomaly that extends to ca. 150 km depth. The Pantanal and Chaco basins are underlain by low velocity anomalies within the upper mantle, locally extending down to 350 km. A high velocity anomaly is associated to the Nazca subducting plate down to 250 km depth; the path coverage impedes deeper vertical resolution. Along the western coast of the South American continent, low velocity anomalies are imaged in the mantle wedge in the regions of "normal" subduction and they are clearly bounded to the north, south and east by high velocity anomalies.

In this paper, we discuss a new 3D shear-velocity model for the upper mantle beneath South America derived from 5850 fundamental and higher mode Rayleigh waveforms analyzed in the period range 50–200 s. Our ray distribution (Fig. 3) provides a dense and homogeneous sampling of the upper mantle, comparable to the one achieved by Vdovin et al. (1999) and superior to that achieved in other regional phase velocity or S-wave models of South-America (Silveira and Stutzmann, 2002; Silveira et al., 1998; Van der Lee et al., 2001, 2002). Compared to Vdovin et al. (1999), the analysis of the full waveform including surface wave higher modes at longer periods allows us to improve the resolution with depth and to build a 3D S-wave model that is less sensitive to crustal effects. We also use a large number of short epicenter-stations paths (Fig. 4) that allow us to resolve horizontal structures with wavelengths smaller than 1000 km (Debayle and Sambridge, 2004). Our results therefore complete previous regional and global tomographic studies in the region by providing a new 3D S-wave model with a much denser and homogeneous coverage of the continent than previous waveform inversion (Van der Lee et al., 2001, 2002) and a better vertical resolution of structures compared to other studies that have been restricted to the fundamental mode of surface waves (Silveira and Stutzmann, 2002; Silveira et al., 1998; Vdovin et al., 1999).

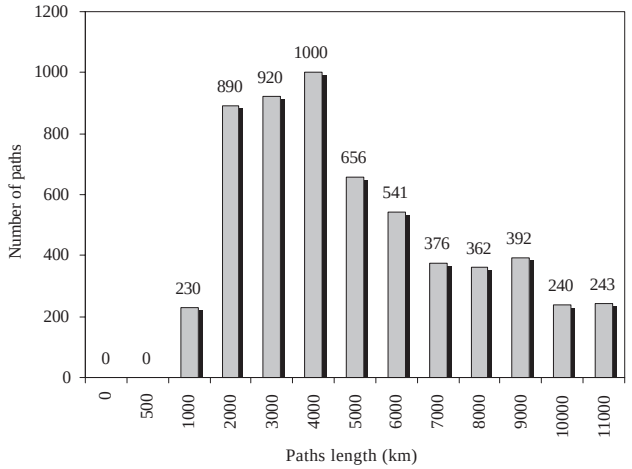

Fig. 4. Number of paths vs. path length: 74.9% of our paths correspond to epicenter-station distances between 2000 and 7000 km.

2. Data selection

Fundamental and higher modes Rayleigh wave seismograms have been recorded at 103 seismological stations (Fig. 5) including 43 IRIS and GEOSCOPE permanent stations, mainly located in South America and Africa, and 60 broadband stations temporarily deployed in northern Chile (APVC experiment, Wal-

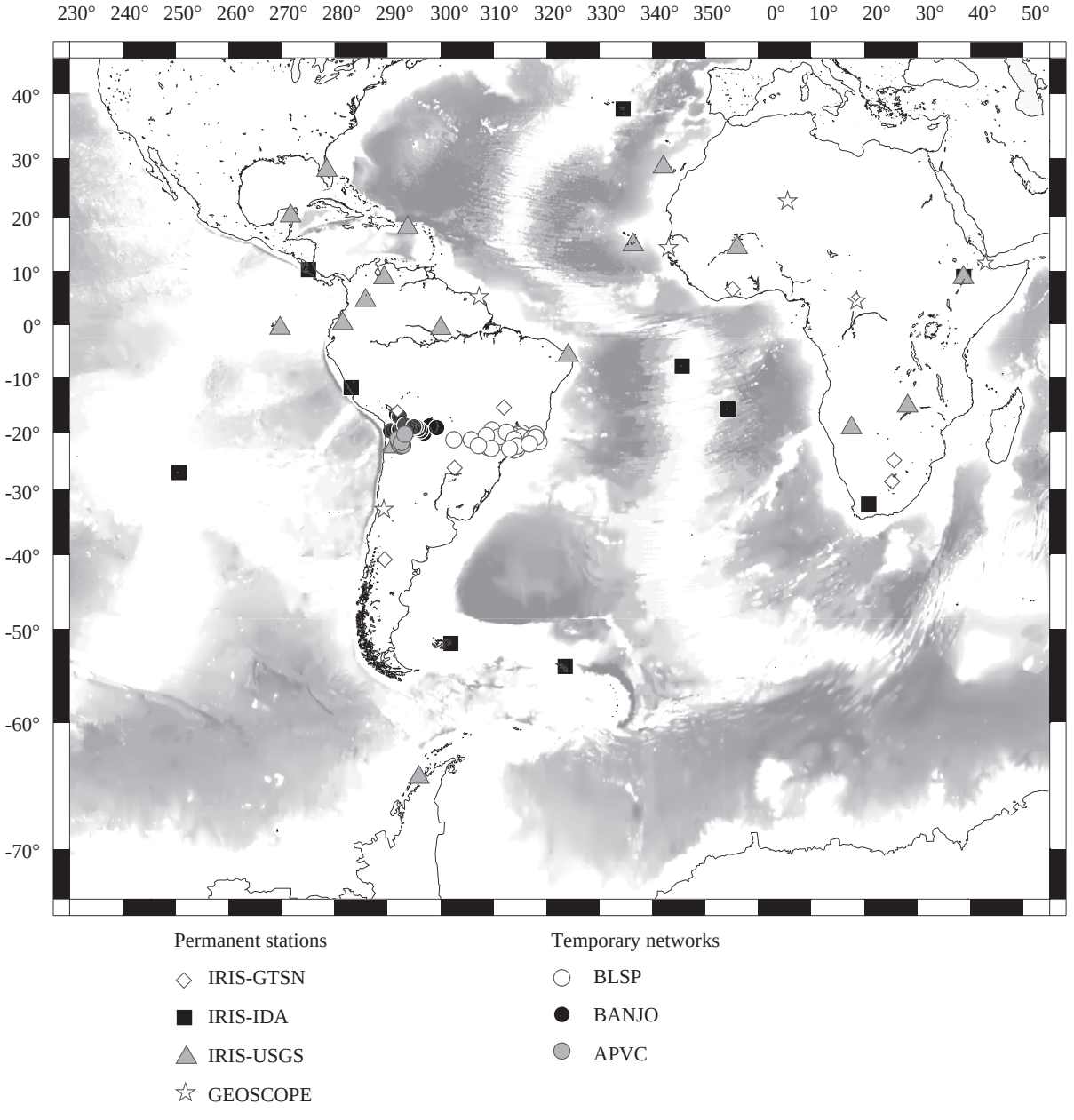

Fig. 5. Location of the seismological stations from which data were used to build the tomographic model. The different symbols correspond to the networks, either permanent stations or temporary deployments: BLSP (Brazilian Lithosphere Seismic Project; James et al., 1993), BANJO (Broadband ANdean JOint experiment; Beck et al., 1996) and APVC (Altiplano-Puna Volcanic Complex; Wallace et al., 1997).

lace et al., 1997), southern Bolivia (BANJO experiment, Beck et al., 1996) and southeastern Brazil (BLSP experiment, James et al., 1993). We selected 1368 events occurring between 1987 and 1999, with a Centroid Moment Tensor (CMT) determination from the Harvard catalogue. Most of these earthquakes are shallow events associated with the Mid-Atlantic, East Pacific, Chile and Carnegie ridges. Deep earthquakes with well excited overtones occurred in the Nazca subduction zone and the Sandwich Islands trench (Fig. 6).

The waveforms of 5850 Rayleigh wave seismograms showing a good signal-to-noise ratio have been successfully matched using an automated version (Debayle, 1999) of the Cara and Lévêque (1987) waveform inversion (see Section 3). This approach allows us to model the fundamental mode and several higher modes, assuming that modes propagate independently without any interaction along the great circle. These assumptions are valid in the period range between 40 s and 300 s for long period surface waves that can be represented with a limited number

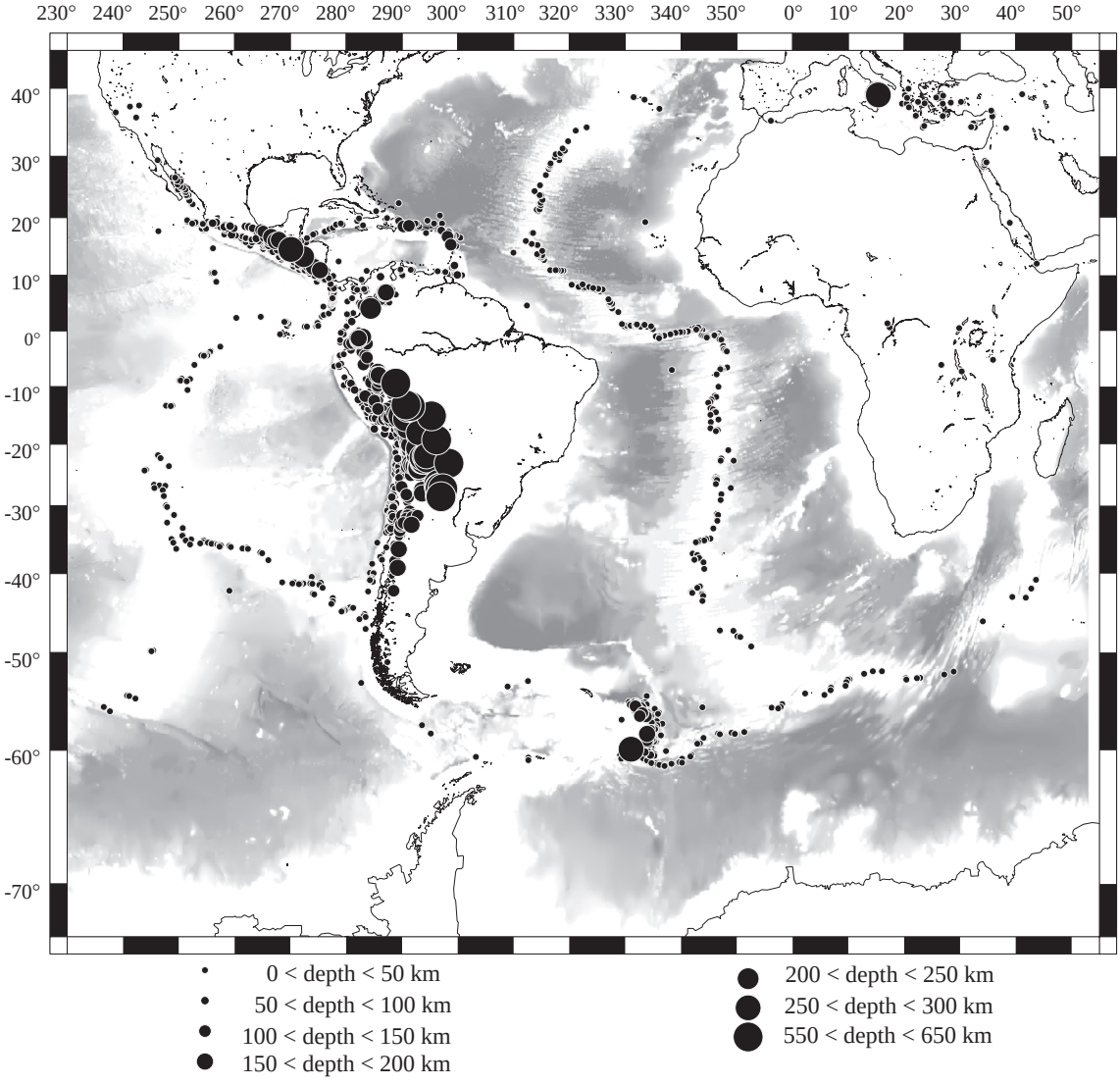

Fig. 6. Epicenter location map. The size of circles is proportional to the depth of the earthquakes.

of modes and correspond to path lengths of few thousands of kilometres (see e.g. Kennett, 1995; Trampert and Woodhouse, 1995). In this study, we stay within the limits of the validity of the theory used for the analysis by modelling waveforms corresponding to paths with typical lengths of about 4000 km (74.9% of our paths correspond to epicenter-station distances between 2000 and 7000 km) in the period range 50–

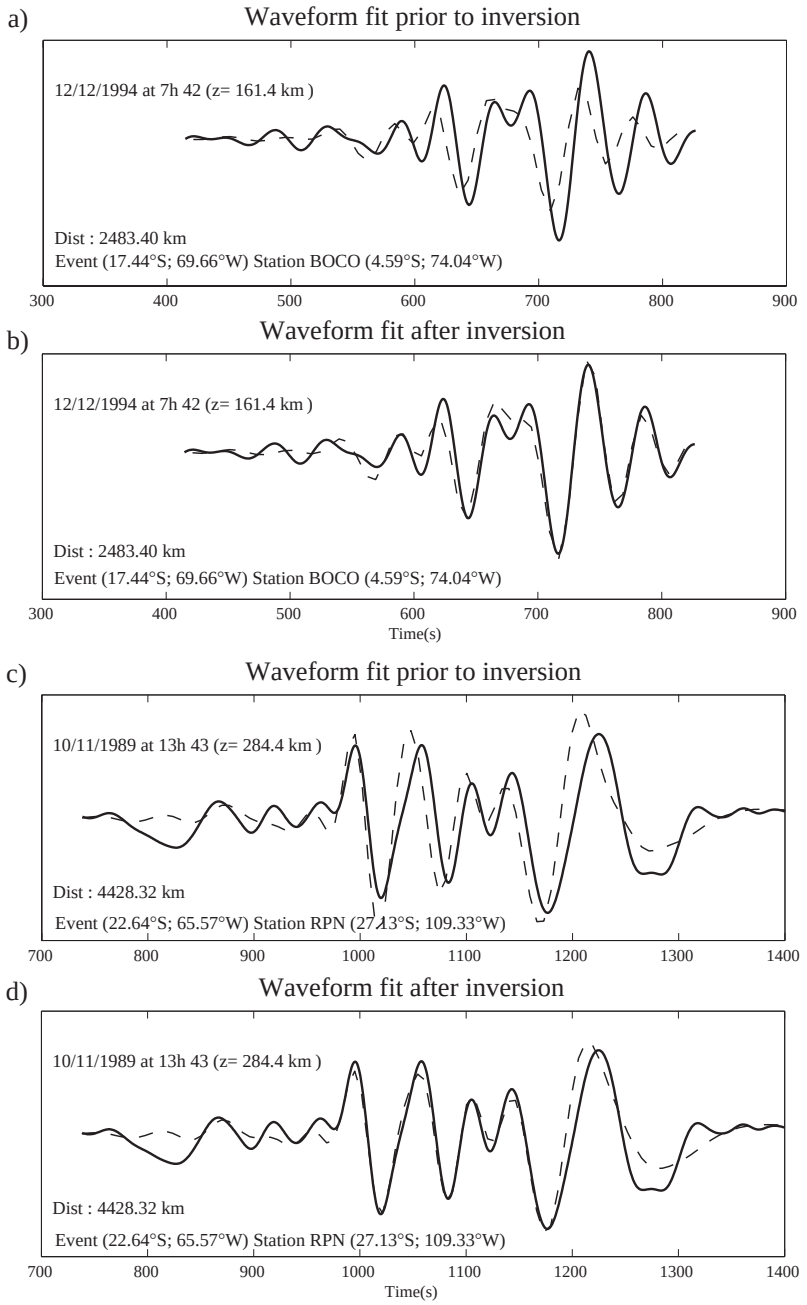

Fig. 7. Example of waveform fit prior (a and c) and after inversion (b and d) for a continental (a and b) path recorded at station BOCO and an oceanic (c and d) path recorded at station RPN. Synthetics are represented as dashed lines, waveforms from real data are shown with solid lines.

160 s and by restricting the modelling to the fundamental mode and up to the fourth higher mode.

The fundamental mode was used in the inversion for 5773 waveforms, and higher modes of order 1, 2, 3 and 4 were included for 1895, 1861, 2737 and 1464 seismograms, respectively. All the waveforms have been inverted for the minimum period range (50–100 s) imposed by the automated modelling (see Debayle, 1999) although periods up to 160 s have been included for 2613 seismograms, generally recorded at the permanent stations which provide a better signal-to-noise ratio at longer periods. The automated procedure allows us to considerably improve the ray coverage by processing an amount of data much larger than compared to "manual" waveform modelling (5850 waveforms in this study against 554 in Van der Lee et al., 2001 where the analysis is not automated). However, to avoid artefacts in the modelling (waveform not properly matched, presence of noise or non-convergence of the non-linear inversion scheme) the thresholds to accept a seismogram are very high. We refer the reader to Debayle (1999) for a detailed description of these thresholds which are based on signal to noise criteria, the quality of the waveform fit and stability of the inversion. Ray density maps for the fundamental and higher modes are displayed in Fig. 3 and show that the South American continent is in general well covered. Up to 400–500 rays cross in the 400×400 km cells located in the black triangle of Fig. 3 and the minimum number of rays remains greater than 100 for the 400×400 km cells in Patagonia and northeastern Brazil.

3. Building the tomographic model

We followed the two-step procedure described in Debayle (1999) which has been previously applied to Australia (Debayle and Kennett, 2000b, 2003), northeastern Africa (Debayle et al., 2001), northeastern Asia (Priestley and Debayle, 2003) and Antarctica (Sieminski et al., 2003). We refer to these papers for a detailed presentation of the method and focus here on the choices specific to this study.

First, using the automated version (Debayle, 1999) of the Cara and Lévêque (1987) waveform inversion approach, we computed multi-mode synthetic seismograms to match recorded waveforms (an example of waveform fit between synthetic and actual data is shown Fig. 7). The source parameters needed to compute the synthetics were extracted from the Harvard catalogue, and the stress-displacement functions required to compute the source excitation functions were computed using the velocity structure provided by the 3SMAC a-priori model (Nataf and Ricard, 1996) in the epicenter region. The procedure allows us to discard seismograms when it is likely that the initial phase at the source is not stable with respect to small perturbations in the path azimuths. Waveform inversion was performed for upper mantle structure only, using a smoothed version of PREM (Dziewonski and Anderson, 1981) as a starting model (Fig. 8). The crustal structure is not inverted, but to avoid bias of crustal origin in the inverted mantle model, corrections are performed by averaging the crustal structure within the 3SMAC model (Nataf and Ricard, 1996) along each source-receiver great circle path. This waveform analysis provides a 1D model of radially stratified upper mantle structure compatible with the recorded waveform for each epicenter-station path.

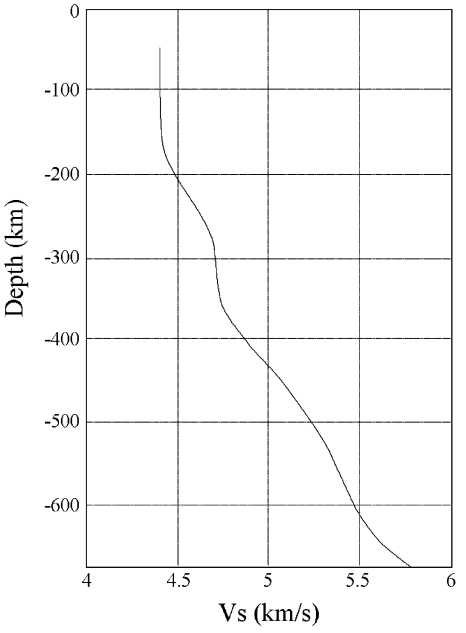

Fig. 8. Smoothed version of PREM used as the starting model for the inversion procedure.

The second step consists in combining the 1D path-averaged models in a tomographic inversion. We used the continuous regionalization algorithm of Montagner (1986) to retrieve the local structure. In this algorithm, the horizontal smoothness of the model is constrained by correlating neighboring points using an a-priori Gaussian covariance function $C_{m0}(r,r')$ defined as:

$$C_{m0}(r,r') = \sigma(r)\sigma(r')\exp\left(-\Delta_{rr'}^2/2L_{corr}^2\right)$$

where $\Delta_{rr'}$ is the distance between geographical points r and r', L_{corr} is the horizontal correlation length which controls the degree of horizontal smoothing in the inverted model and $\sigma(r)$ and $\sigma(r')$ are an a-priori standard deviation which controls the amplitude of the perturbations in the inverted model at each geographical point r. After several trials we chose a value of 400 km for L_{corr}. This value corresponds to the wavelength of a surface waves at about 100 s period and is chosen such as the overlap between the surface of width $2L_{corr}$ centered around each of the ray paths ensures a good coverage of the studied area. Our tomographic result is non-unique. For example, changing the value of L_{corr} by a factor of two would result in more or less detailed tomographic images but would not change the main outcomes of the tomographic results discussed here. The a-priori standard deviation was taken equal to 0.05 km s^{-1}; this corresponds to commonly observed SV-wave velocity variations (Debayle and Lévêque, 1997; Nishimura and Forsyth, 1989).

4. Possible artefacts

Several effects may produce artefacts in the 3D S-wave tomographic model. These include approximations used in the theory, or a poor knowledge of some of the parameters which are not included in the inversion such as the crustal structure along the paths and the focal mechanism at the source. The procedure allows us to minimize spurious effects due to a poor knowledge of the source parameters by discarding seismograms when it is likely that the initial phase at the source is not stable with respect to small perturbations in the path azimuths. For those paths that pass the selection tests, these effects have no reason to be coherent since they are related to events with different focal mechanisms and different focal depths, they are therefore expected to be averaged out by our azimuthal coverage in the tomographic inversion.

Crustal effects are also not expected to affect significantly our results. Debayle and Kennett (2000a) discuss the effects of changing the average crustal thickness along the path by 10 km for a path crossing the Australian continent. An error of 10 km on the path averaged crustal thickness is likely to represent an upper bound for crustal effects, as a 200 km wide zone with a 10 km difference in crustal thickness will only produce a difference of 2 km in the average crustal model for paths as short as 2000 km. However, Debayle and Kennett (2000a) found that the perturbation on the resulting path average shear velocity model exceeds the error bars only in the uppermost 100 km of the mantle. For South America, the crustal structure provided by the 3SMAC model (Nataf and Ricard, 1996) differs locally from the CRUST2.0 model of Laske et al. (2000: http://mahi.ucsd.edu/Gabi.rem.html) (Fig. 9a and b). Since these differences are very localized and do not exceed $2\times2^\circ$ cells, it is unlikely that once averaged along the epicenter-stations paths, they may significantly affect our long period surface waves whose maximum sensitivity at 50 s period is located below the Moho at 75 km depth. The Moho depth in the 3SMAC model has a closer correspondence to the different geological domains (basins or cratons) known from the surface geology of South America (Fig. 9a and b). It is also in better agreement with recent receiver functions results in the Amazonian region (Krüger et al., 2002) showing a variation of the Moho depth from 38 km under the basin to 48 km northward. The 3SMAC model was therefore used to perform crustal corrections, although using the CRUST2.0 model would not change significantly the results presented in this paper. Indeed, both the good agreement found between the recent global models based either on the 3SMAC model (Debayle et al., 2005) or on the CRUST2 model (Ritsema et al., 1999), and the direct comparison of the two crustal models performed by Pilidou et al. (2004), confirm that the choice of the 3SMAC or CRUST2 crustal model has little effects on the upper mantle model at depths greater than 100 km. In this paper, we do not discuss the part of

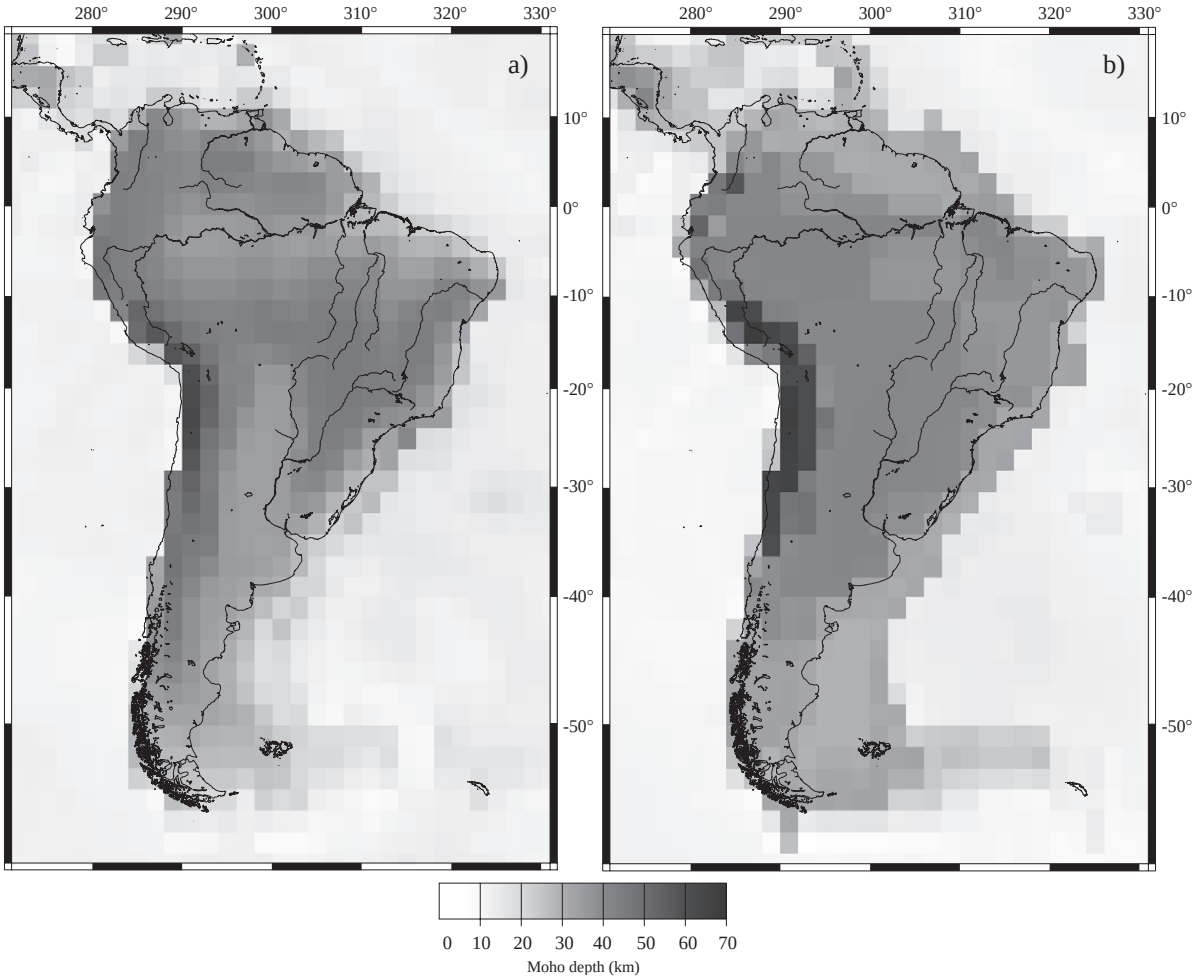

Fig. 9. Comparison of the Moho depth between (a) the 3SMAC and (b) CRUST2.0 models.

our model lying at depths shallower than 100 km where crustal effects could be more important.

5. Synthetic experiments

In this section, we present several synthetic experiments to check our ability to retrieve heterogeneities with horizontal wavelengths of several hundred of kilometres, located at various depths and in various locations of our tomographic model. Our input velocity model at all depths is the S-wave velocity distribution extracted at 50 km depth from the 3SMAC (Nataf and Ricard, 1996) a-priori Earth model to which we add additional perturbations. The 3SMAC model provides a realistic distribution of input velocities for the upper mantle (e.g. high velocity anomalies are correlated with cratonic roots and low velocity anomalies are linked to South Atlantic and East Pacific ridges) but remains sufficiently different from the output of the actual inversion to allow us to discuss the synthetic results. In each simulated experiment the inversion is performed using exactly the same ray coverage and the same a-priori information as in the actual inversion. In particular, as in Debayle et al. (2001), the weight given at each depth to each 1D path average model depends on the a-posteriori error determined after the actual waveform inversion. This a-posteriori error is large at a given depth when the actual waveform contains little information related to

the corresponding structure. In this way, these synthetic tests carry the depth sensitivity of the actual dataset. The 5850 synthetic seismograms are then inverted following the same automated procedure as for actual data.

The first test (Fig. 10a) is designed to check our ability to isolate an anomaly located at different depths under the Altiplano-Puna plateau in the Andean Cordillera. A −5% velocity perturbation is added to the a-priori 3SMAC input model within a ~800 × 400 km region elongated north–south and centered at (22°S; 294°E). The output models at 100 and 150 km depth show that the geometry of this anomaly is satisfactorily recovered although its amplitude is attenuated (~34% and ~26% of the input anomaly are recovered at 100 and 150 km depth, respectively).

Similarly, the geometry of a +5% shear-velocity anomaly located below the Andean Cordillera in the continuity of the Carnegie ridge (extending between 282°E and 286°E longitude and between 6°N and 2°S latitude) is well recovered between 100 and 200 km depth (Fig. 10b). The amplitude recovery decreases with depth from ~75% at 100 km to about ~59% at 200 km depth. Similar conclusions have been obtained for an anomaly located at the intersection between the Chile ridge and the continent (not shown). The geometry is correctly resolved, although the amplitude recovery is weaker due to a sparser ray coverage at the southern tip of the continent (Fig. 3). Down to 350 km depth beneath the Guapore shield (Fig. 10c), still ~19% of a +5% shear-velocity anomaly imposed in the input model is recovered. This suggests that the structure beneath the Amazonian craton is well resolved in our 3D shear-velocity model.

We performed other synthetic tests (an example is provided in Fig. 10d, where a −5% shear-velocity anomaly centered on 3°S latitude and extending between 301°E and 305°E longitude, from 75 to 150 km depth is injected in the starting model) which confirm that in the well covered part of our model, deeper structures are retrieved down to 350 km depth providing that their lateral extension exceeds few hundred of kilometres with a velocity contrast greater than few percents.

This series of simulated experiments suggests that we are able to satisfactorily recover velocity anomalies in the uppermost 350 km of the South American continent, provided their lateral extension and velocity contrast reach several hundred of kilometres and a few percents, respectively. The amplitude recovery depends on the horizontal extent of the input anomalies. In Fig. 10a, b, c and d, long wavelength structures (high velocities beneath the cratons or low velocities beneath the western coast of South America) are better recovered than the short wavelength anomalies that we added to the 3SMAC model. The velocity anomalies discussed in this paper have horizontal wavelengths of several hundred of kilometres and contrasts with neighbouring structures greater than 2%. This suggests that these anomalies reliably represent mantle velocity heterogeneities.

6. Results

The 3D velocity model resulting from the surface wave inversion is presented in Fig. 11 as a set of maps displaying S-velocity perturbations at 100, 150, 200, 250 and 300 km depth (Fig. 11a–e) together with two cross-sections at 20°S latitude and 305°E longitude (Fig. 11f). Velocity perturbations are shown relative to the reference velocity indicated on the maps. The Montagner's (1986) regionalization algorithm is based on the inversion scheme developed by Tarantola and Valette (1982) and allows us to compute the a-posteriori covariance matrix which provides an evaluation of the quality of the inverted model. Note that in the Tarantola and Valette (1982) formulation, the a-posteriori covariance matrix incorporates the covariance matrix on the data (e.g., see Montagner, 1986 or Debayle and Sambridge, 2004 for the expressions of the a-posteriori covariance and resolution in the case of the surface wave problem discussed here). The a-posteriori covariance matrix C_m is related to the a-priori covariance matrix C_{mo} by the relation $C_m = (I-R)C_{m0}$, with I as the identity matrix and R as the resolution matrix. The a-posteriori error or standard deviation are the square roots of the diagonal terms of the a-posteriori covariance matrix C_m. It is therefore clear that when the resolution is null the a-posteriori error will be equal to the a-priori error while for perfect resolution (i.e. $R=I$), the a-posteriori error should be null. The "true" model has 68% of chance to lie within one a-posteriori error of the inverted

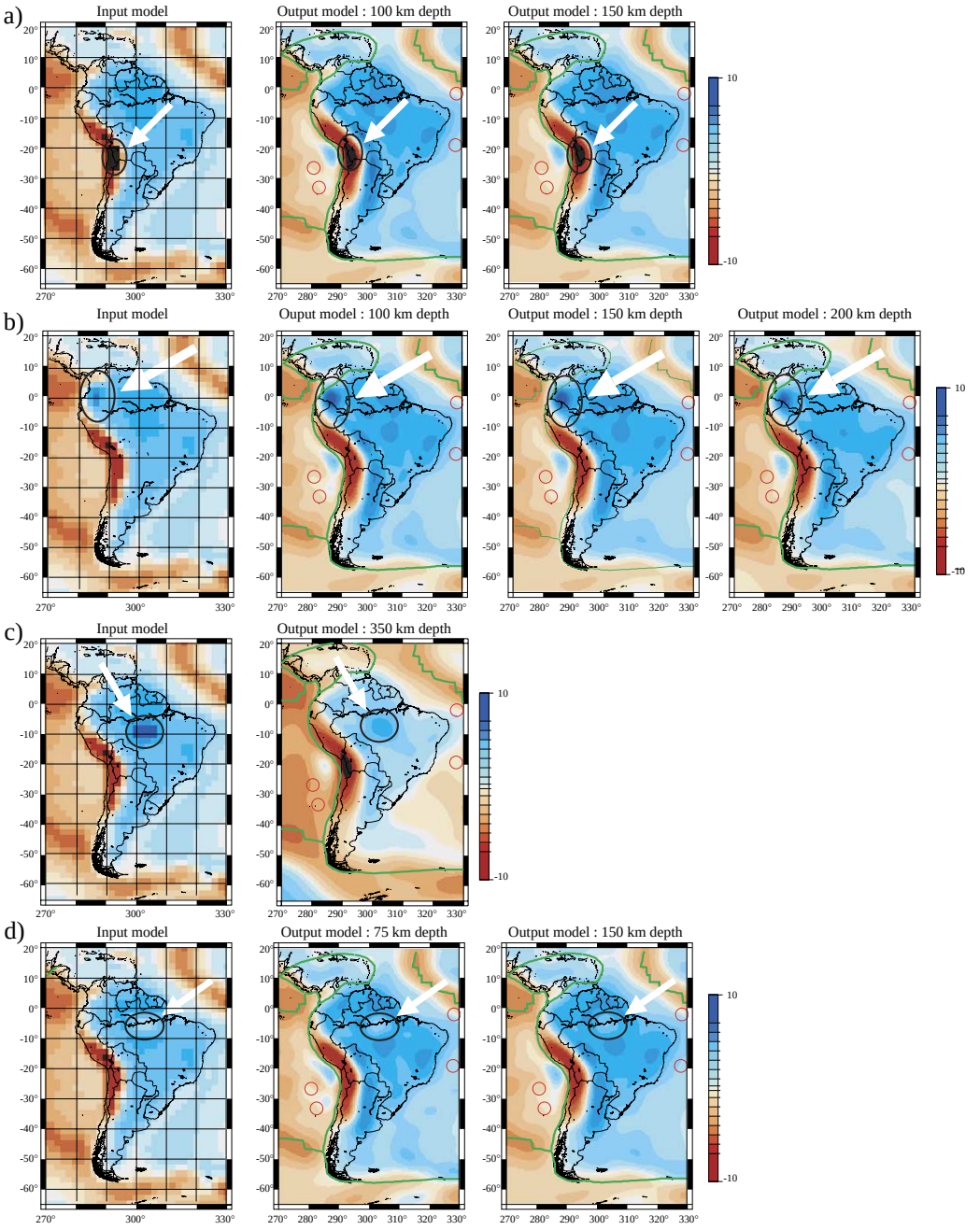

Fig. 10. Synthetic experiments to check the ability to retrieve heterogeneity with horizontal wavelengths of several hundred of kilometres, located at various depths and in various locations of our tomographic model. The left column shows the input velocity model, which is the S-wave velocity distribution extracted at 50 km depth from the 3SMAC a-priori Earth model. Perturbations have been added to the input model: (a) a low velocity anomaly located beneath the Altiplano-Puna plateau, (b) a low velocity anomaly related to the subduction of the Chile ridge beneath the South American continent, (c) the depth extent of the high velocity anomaly located beneath the Guapore craton, (d) a low velocity anomaly beneath the Amazon basin, accounting for a separation into two blocks of the Amazonian craton. For each experiment, the output model is shown at different depths.

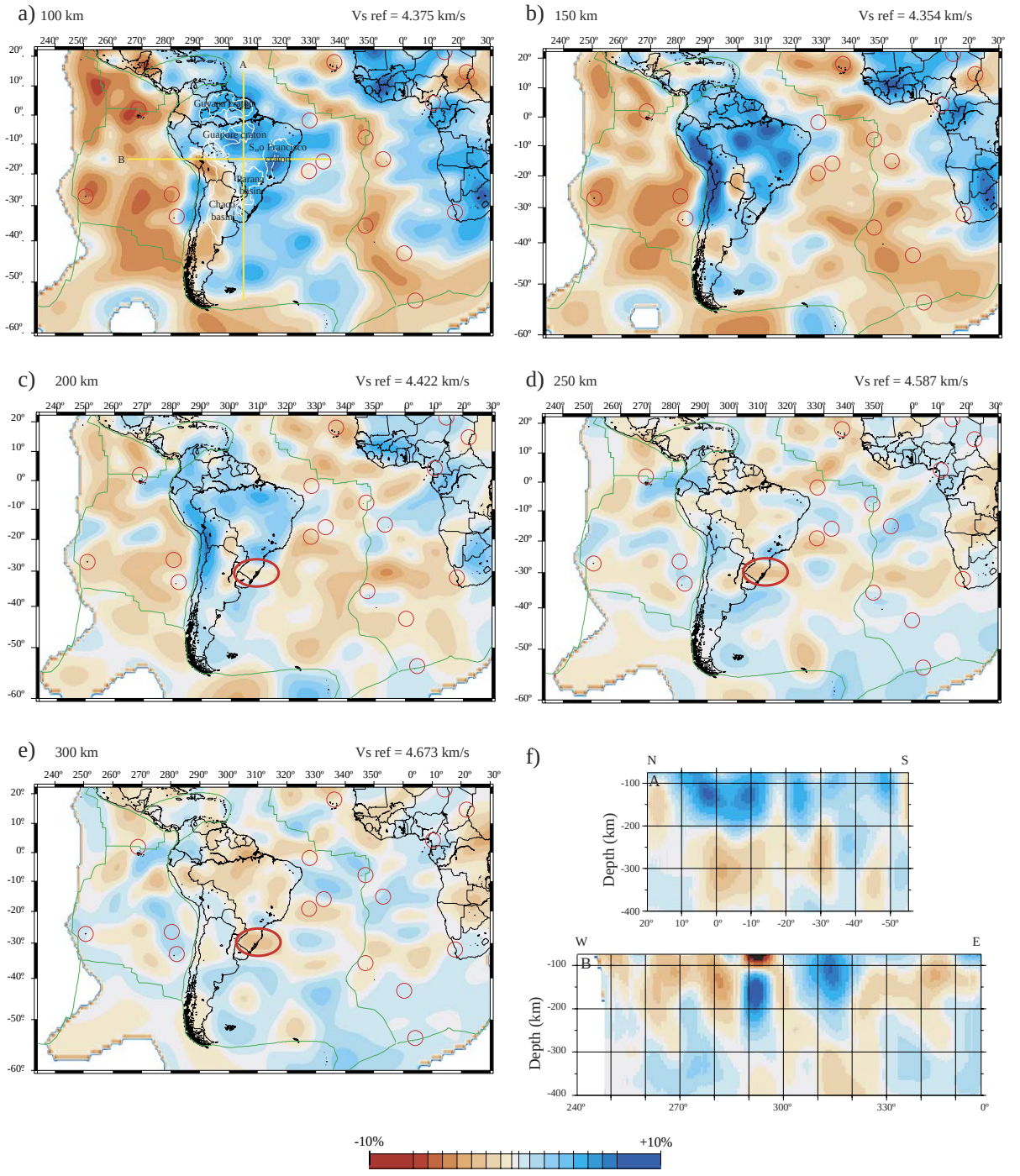

Fig. 11. SV wave heterogeneity maps at 100 km (a), 150 km (b), 200 km (c), 250 km (d) and 300 km (e) depth with two cross sections (f) at 305°E longitude (A) and 20°S latitude (B). For each map, the hotspots are plotted as open circles, and the tectonic plates are delimited by green lines. Regions in white correspond to areas with a lack of resolution. The red circle on figures c, d and e, outlines the low velocity anomaly imaged under the Paraná large igneous province discussed in the text.

model and 95% of chance to lie within twice the a-posteriori error.

Fig. 12 shows maps and cross sections corresponding to those presented in Fig. 11 but for the a-posteriori error model built from the diagonal terms of the a-posteriori covariance matrix. Dark gray areas on the borders of the maps correspond to regions where the a-posteriori error is close to the a-priori error and indicate a lack of resolution. Light gray regions correspond to areas where the a-posteriori error is significantly smaller than the a-priori error (threshold fixed at 0.04 km s^{-1}, i.e. 80% of the 0.05 km s^{-1} a-priori error) indicating that resolution is good. The best resolved areas, with the smallest a-posteriori errors, are located beneath the western coast of South America where the highest ray density is available. Although resolution decreases with depth as indicated by the increase of the a-posteriori error in Fig. 12, the western coast of South America corresponds to the best resolved area in the deeper parts of the model, thanks to the occurrence of deep events with well excited overtones. The 95% confidence level in the results corresponds to two standard deviations or twice the a-posteriori error. This means that in regions where the a-posteriori error reaches 0.04 km s^{-1}, velocity contrast smaller than 1.6% should not be interpreted. However, it is commonly accepted in the literature that the 68% confidence level (one standard deviation) is meaningful. This would allow us to interpret velocity contrast of at least 1% in most regions of the tomographic maps, down to at least 300 km depth.

For simplicity sake, the presentation of the tomographic model is split into three main parts related to the main geodynamical domains: the oceanic basins, the Pacific active margin, and the continental domain.

6.1. The oceanic basins

The eastern part of the Pacific Ocean and the South Atlantic Ocean from 20°N to 60°S are well resolved (Fig. 12). In both oceanic domains, the oceanic ridges (East Pacific, Chile, Cocos and Carnegie ridges in the Pacific Ocean and the Mid-Atlantic ridge, Fig. 2a) are associated with low velocity anomalies at depths shallower than 150 km. The width of the negative velocity anomalies associated with the ridges in the Pacific and Atlantic oceans are however significantly different. At 100 km depth (Fig. 11a) the low velocity anomaly associated to the Mid-Atlantic ridge is narrower compared with the broad low velocity anomaly underlying the eastern Pacific ridges and most of the Nazca plate. This difference is related to the contrasting spreading rates of the fast Pacific ridge and the slow Atlantic ridge (Fig. 2c): young, hot and thin oceanic lithosphere spreads at larger distances from ridges in the Pacific than in the Atlantic.

At 100 km depth (Fig. 11a), low velocity anomalies are located beneath the Easter Island and Galapagos hotspots in the Pacific Ocean and the Cap Verde, Ascension, Saint Helen, Trinidad and Tristan da Cunha hotspots in the Atlantic Ocean (see Fig. 2a for location). This suggests the presence beneath these hotspots of a broad region (500–1000 km) of anomalously hot material at this depth, which may result from thermal erosion of the oceanic lithosphere (e.g., Parmentier et al., 1975) by mantle plumes. This conclusion is supported by the recent finite-frequency tomography of Montelli et al. (2004), revealing a variety of plumes in the deep mantle beneath the Atlantic and Pacific oceans, located beneath these hotspots. However, at depths larger than 100 km where the plume anomaly could be related to a narrower conduit with a diameter of about 100–200 km, long period surface waves may not provide the horizontal resolution to resolve such narrow features. The low velocity anomaly associated with the Galapagos hotspot at 100 km depth has an unusually large amplitude (up to −7.4% at 100 km depth, Fig. 11a) that may reflect a combination of the effects of the Cocos and Carnegie ridges, and of the Galapagos hotspot.

A region with high seismic velocity is observed in the central Atlantic ocean in the depth range 250–400 km. This includes high seismic velocity anomalies located westward of the West African coast and eastward of the Brazilian coast that have been associated by King and Ritsema (2000) with secondary convections on the edge of cratons.

6.2. The Pacific active margin

This region is characterized by dense ray coverage (Fig. 3) and the presence of deep earthquakes providing well excited overtones (Fig. 6). Consequently, the

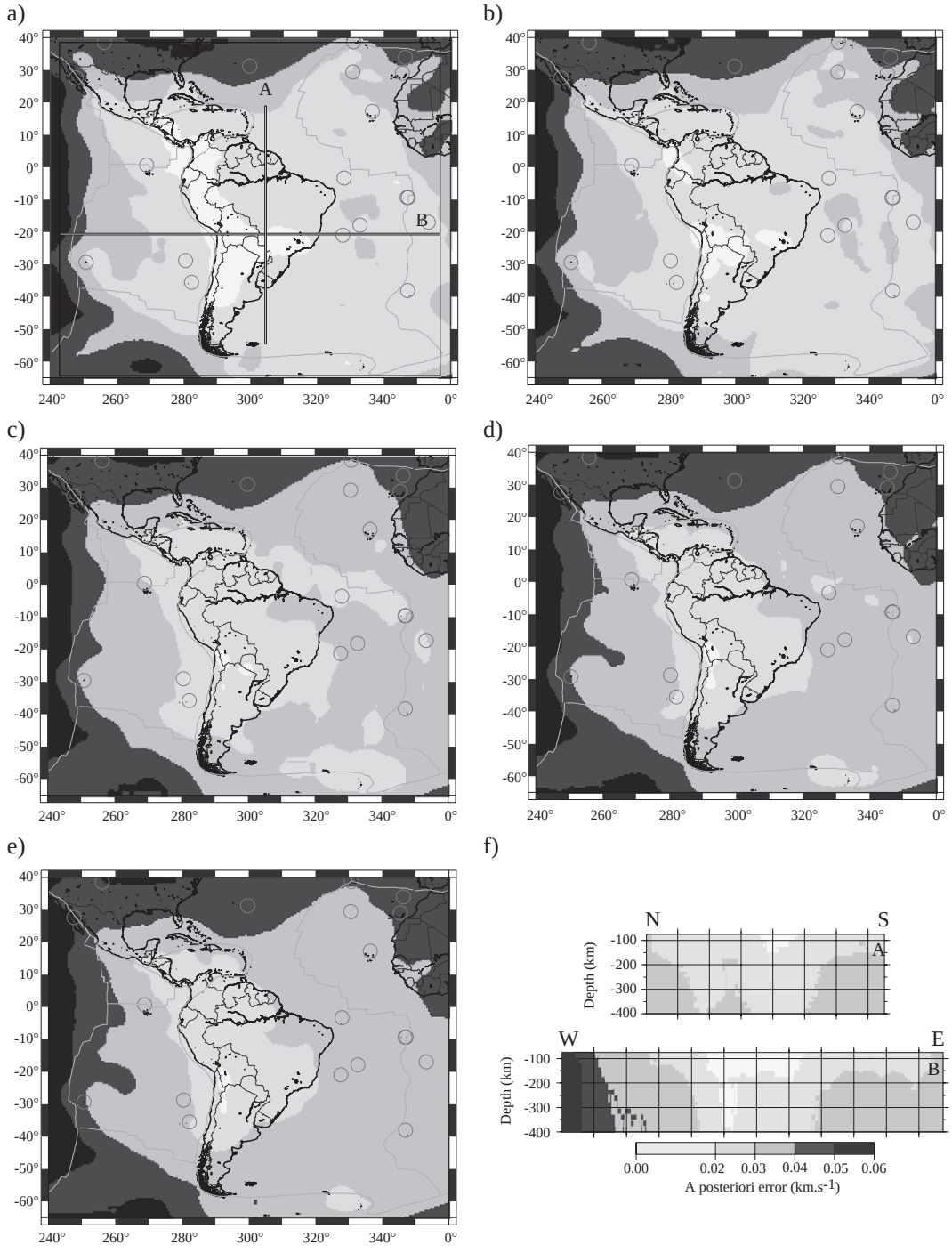

Fig. 12. A-posteriori error maps at 100 km (a), 150 km (b), 200 km (c), 250 km (d) and 300 km (e) depth associated with two cross-sections (f) at 305°E longitude (A) and 20°S latitude (B). Dark grey areas on the borders of the map indicate regions where the a-posteriori error is close to the a-priori error (0.05 km s^{-1}), meaning therefore a total lack of resolution. The best resolved areas, with the smallest a-posteriori errors, are located beneath the western coast of South America, and are well resolved until at least 300 km depth.

a-posteriori error under western South America remains smaller than 0.03 km s^{-1} down to at least 300 km (Fig. 12), suggesting that velocity contrasts larger than 1% can be interpreted. At 100 km depth (Fig. 11a), two longitudinal high velocity anomalies are observed beneath the Pacific active margin between 5°S and 15°S and 22°S and 37°S. They are bounded by two low velocity regions located North of 5°S, extending to 100 km depth, and South of 37°S, extending to 150 km depth. These low velocity regions correspond to the intersection between the South American western coast and the Carnegie and Chile ridges. From 15°S to 22°S latitude, a large low-velocity anomaly (−8%) extends along the Pacific margin down to ca. 130 km depth and is likely located above the subducting slab (Fig. 11a and cross-section B, Fig. 11f). Previous local body-wave tomography found low seismic velocities or high attenuation (Dorbath and Masson, 2000; Haberland and Rietbrock, 2001; Masson et al., 2000; Myers et al., 1998; Schurr, 2001) in this region of active volcanic arc that is also associated with an anomalously high heat flux, around 115 ± 24 mW/m^2 (Hamza and Muñoz, 1996). Partial melting in the mantle wedge, triggered by the release of fluids from the dipping slab when it reaches 100 km depth provides an explanation for the combined observations (Van der Lee et al., 2001, 2002). At 150 and 200 km depth, a continuous high velocity anomaly is observed from 5°S to 37°S. This high velocity anomaly extends down to 300 km depth beneath the central volcanic zone where it exceeds 1%.

6.3. Continental domain

A good correlation exists between the main geological domains of the South American continent and the velocity structure shown in our model. The most striking result is the high velocity lid associated with the main cratons of South America that extends down to about 200 km depth. In the uppermost 150 km, the surrounding Neoproterozoic mobile belts are characterized by seismic velocities closer to the PREM model, and the sedimentary basins are generally associated with low velocity anomalies.

The mantle beneath the São Francisco and the Amazonian cratons is characterized by high shear velocity (+5.9% and +8.2%, respectively at 100 km depth, and +2.2% and +4.8% at 200 km depth) down to a depth of about 200 km (Fig. 11a, b, c). In contrast with previous regional models (Silveira and Stutzmann, 2002; Silveira et al., 1998; Van der Lee et al., 2001, 2002) our model suggests that the high velocity anomaly associated with the Amazonian craton is subdivided in the uppermost 100 km in two domains located beneath the Guyana and the Guapore shields. These two domains are separated by the ENE-trending Amazon and Solimões rift basins, associated at 100 km depth with moderately high seismic velocities (about +3.3%) in our model. The contrast observed at 100 km depth between the Amazon and Solimões basins and the shields is larger than 2% and is thus significant relative to the a-posteriori error in the region. It is also difficult to explain this contrast by crustal effects. As discussed in Section 4, crustal effects are likely to be confined at depths shallower than 100 km. In addition, there is no clear correlation between the 3SMAC crustal map of Fig. 9a and our velocity map at 100 km depth. Although, the EW band of "less high velocities" at 100 km below the Amazon basin is associated with a relatively thinner crust in the 3SMAC model, there is for example, a broad region with similar "less high velocities" at the intersection of the two cross-sections A and B on Fig. 11a which is not associated with a thin crust in the 3SMAC model (Fig. 9a).

In contrast with previous regional model (Silveira and Stutzmann, 2002; Silveira et al., 1998; Vdovin et al., 1999) the high velocity anomaly correlated to the São Francisco craton down to ~200 km depth is clearly distinguished from the one underlying the Amazonian craton. This is in good agreement with the existence of a Neoproterozoic belt between the two cratonic blocks. Southwest of the São Francisco craton, a high velocity anomaly (+4%) extends down to at least 200 km depth under the Paraná basin (Fig. 11a,b,c). Snoke and James (1997) found high shear wave velocity in the uppermost 200 km of the mantle beneath the Paraná basin and normal to low shear velocities in the mantle beneath the Chaco basin. Previous gravimetry (Lesquer et al., 1981) and receiver functions (Snoke and James, 1997) studies also suggested that the lithosphere beneath the Paraná basin and the São Francisco craton might be continuous at depth. Our model confirms that the Paraná basin may be underlain by cratonic lithosphere down to about 200 km as for the São

Francisco craton. The Chaco basin is characterized by normal to low seismic velocities down to 200 km depth.

A major issue addressed by tomographic studies is the depth extent of cratonic roots. In our model, the Amazonian and São Francisco cratons are highlighted by a high velocity anomaly down to 200 km depth. The starting model in the tomographic inversion procedure is a smoothed version of PREM (Fig. 8) showing a moderately high velocity gradient at around 220 km depth and one might wonder about the effect of this starting model on the vanishing of the high velocity anomaly associated to the cratonic roots near 220 km. An important point is that the strength of the horizontal variations observed at each depth is independent of the 1D background model that, at a given depth, is the same everywhere on the map. A robust observation from our model is the decrease in the velocity contrast between cratonic roots and younger tectonic regions. Cratonic roots are in average 10% faster than younger tectonic regions at depths shallower than 220 km while at larger depths this difference is strongly attenuated. This decrease in the lateral distribution of seismic contrasts cannot be attributed to the 1D depth-dependent starting model because at each depth, the background velocity is the same everywhere on the map, and the accuracy of horizontal contrasts retrieved by the model is not affected by the value of the background model. In other words, the vanishing of the seismic difference between cratonic roots and younger tectonic provinces near 200 km cannot be attributed to the starting model.

From 200 to 375 km depth, a localized low velocity anomaly persists under the southern part of the Paraná basin. This anomaly is located below the Ponta Grossa arc, an ancient volcanic region probably related to the passage of the Tristan Da Cunha hotspot (Turner et al., 1994). The anomaly extends into the Atlantic domain where it roughly follows the trace of the plume. This low velocity anomaly is located 800 km south of a low velocity anomaly found between 200 and 500–600 km depth in P- and S-wave traveltime tomography for the Paraná basin (Schimmel et al., 2003; VanDecar et al., 1995). The large geographical distance between these two anomalies suggests that they may not be correlated. Nevertheless, the LIP associated to the Paraná basin is so widespread that the anomaly highlighted in our tomographic model may still be linked to the surface expression of the Tristan da Cunha plume head.

7. Discussion

In the uppermost 150 km of our model, the high velocity anomaly associated to the subducted Nazca plate is bounded by two low velocity anomalies located beneath the continental margin at the continuation of the Carnegie and Chile ridges. These low velocity anomalies underlying young oceanic lithosphere (compare Figs. 11a and 2c) may represent the thermal signature of subducted ridge segments. In both regions, the seismicity is rather shallow, extending no deeper than 150 km depth at the latitude of the Carnegie ridge and 33 km depth in the neighborhood of the Chile ridge. In contrast, along the central part of the Cordillera, earthquakes are observed down to 650 km depth (Figs. 2b and 6). The volcanic activity is also reduced above the subducted ridges (Gansser, 1973). Moreover, while most of the Andean volcanoes are andesitic in character, adakitic magmatism has been documented near the Chile triple junction (CTJ) both on the continent (Martin, 1999) and within the trench (Lagabrielle et al., 2000). Modern adakites bear geochemical characteristics (high Sr, Cr, La/Yb, Sr/Y especially) suggesting that they derive from melting of an abnormally hot subducted oceanic crust. This may arise when the subducted slab is young, or when it has resided a long time in the mantle, e.g., shallow or subhorizontal subduction (Davaille and Lees, 2004). Adakitic rocks, ranging in age from about 1.5–6 My, are present 10–50 km south of the CTJ, in areas where the margin and the subducting ridge have been interacting since 6 My. There is a clear correlation between the emplacement of these magmas and the migration of the CTJ along the margin (Lagabrielle et al., 2000). Due to the special plate geometry in the CTJ area, a given section of the margin may be successively affected by the passage of several ridge segments, leading to the development of very high thermal gradients and to a strong and long-lived thermal anomaly (Fig. 13). This hypothesis is in good agreement with the low velocity anomalies observed in our model and with heat flux measurements (Hamza and Muñoz, 1996): heat flow values up to 160 mW/m^2 have been measured along the Patagonian Cordillera

and in the Central Valley, whereas values around 33 mW/m^2 are measured along the coastal Cordillera, and 100–115 mW/m^2 along the Pampean Ranges and in the Tamarugal Plains (Fig. 13).

The subduction of the Chile ridge is also associated with a variation of the dip angle between the subducting Nazca and Antarctic plates at the CTJ (Fig. 13a). The subduction of the Antarctic plate beneath the South American continent has a shallow dip (Fig. 13b) whereas the Nazca plate in this region is dipping ~30° (Fig. 13c). This difference in dip angle on both sides of the subducted ridge suggests that it has been

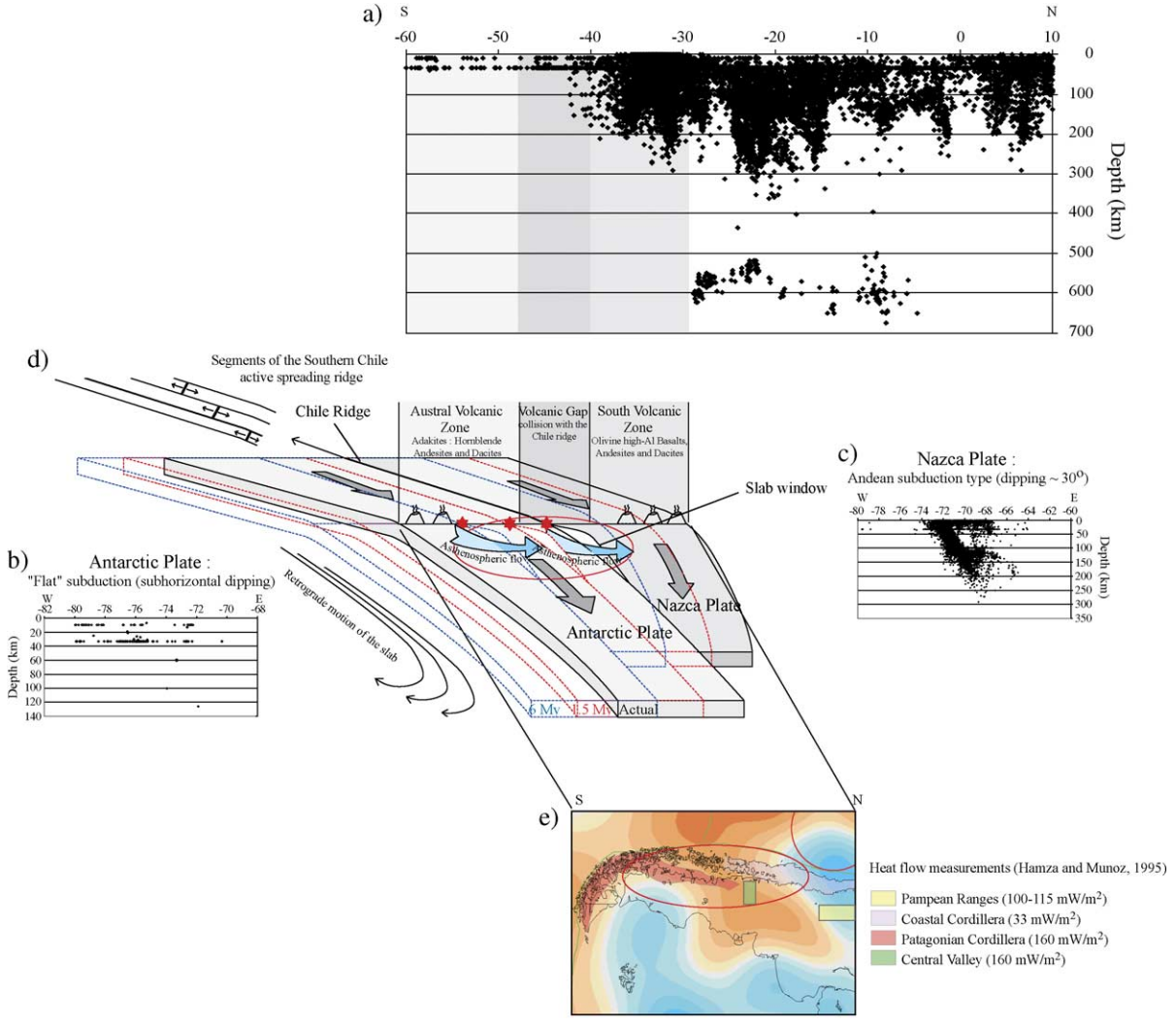

Fig. 13. 3D block diagram showing the migration of the Chile triple junction along the western margin of the South American continent and the development of a slab window allowing mantle to flow from the Pacific to the Atlantic oceanic basin. Three cross-sections show the distribution of seismicity with respect to depth, (a) from 10° to 60°S latitude along the western coast of the continent, (b) from −82°E to −68°E beneath the Antarctic plate and (c) from −80°E to −60°E longitude beneath the Nazca plate. A given section of the margin can be successively affected by the passage of several ridge segments (d), leading to the development of very high thermal gradients and to strong and long-lived thermal anomalies, as shown by measurements performed by Hamza and Muñoz (e). Red stars represent adakites dredged in the trench at different localities (Lagabrielle et al., 2000).

progressively "unzipped", forming a slab window (Dickinson and Snyder, 1979)–a kind of tear in the slab–allowing hot mantle from beneath the slab to flow across the slab (Fig. 13). This model is supported by the decrease of the volcanic and seismic activities approaching the intersection between the ridges (Chile to the south and Carnegie to the north) and the trench. A similar model has been proposed for the Cocos-Nazca subduction which may also have resulted in the development of a slab window beneath Central America (Johnston and Thorkelson, 1997). Similarly, tomographic images of the distribution of shear-wave velocities beneath the northwestern Pacific, and more precisely beneath Kamchatka, led Levin et al. (2002, in press) to suggest that the segment of the Aleutian Arc extending between 164°E and 173°E overlies a portal in an otherwise continuous lithospheric slab. In agreement with the previous study, simple thermal modelling performed by Davaille and Lees (2004) accommodates the seismicity shoaling together with the increase of the heat flow and presence of unusual volcanic products related to adakites at the Aleutian-Kamchatka juncture by a tear in the oceanic lithosphere along the northern edge of the Pacific plate (Davaille and Lees, 2004). A final example of slab window is the one reported by Smith et al. (2001) in the subducting Pacific plate, allowing mantle from the Samoan plume to flow parallel to the trench into the Lau basin.

The low velocity anomalies associated with the subduction of the Chile and Carnegie ridges allow us to propose an alternative model of mantle flow to the one suggested by Russo and Silver (1994): from shear-wave splitting measurements, they determine the anisotropy pattern of the mantle beneath the subducting Nazca plate, Cocos plate and Caribbean region. Assuming a retrograde motion of the Nazca slab and decoupling between the slab and the underlying asthenospheric mantle, the mantle flow induced by this movement should be three-dimensional with a trench-parallel flow component, in agreement with the direction of polarization of the fast split shear wave. This trench parallel flow is supposed to diverge northward and southward from a stagnation point located at ca. 20°S latitude. Considering that the Pacific ocean is surrounded by retrograde slab motions, the mass conservation between the Atlantic and Pacific oceans might therefore be accommodated by a flow of asthenospheric mantle from the shrinking Pacific basin to the expanding Atlantic one. Russo and Silver (1994) suggested that the asthenospheric mantle would flow around both tips of the continent. Using teleseismic shear-wave splitting as a tool to investigate mantle flow around South America, Helffrich et al. (2002) however disagreed with Russo and Silver (1994); their results show no evidence for present-day flow around the tip of southern South America, but instead present-day flow directions in the southern Atlantic that parallel the South American absolute plate motion direction.

Considering the low velocity anomalies correlated in our velocity model with the subducted Carnegie and Chile ridges, together with the variation in the subduction angle from normal to subhorizontal on both sides of the two subducted ridges, we suggest an alternative model in which the sublithospheric mantle flow from the Pacific to the Atlantic basins is channeled by the slab windows opened along the subducted ridges.

Geological and geochronological similarities in the Guyana and Guapore shields led Tassinari and Macambira (1999) to suggest that the Amazonian craton was initially a single microcontinent which was split during a rifting episode that resulted in the development of the Amazon and Solimões basins. The Amazon basin covers 500,000 km^2 and merges westward with the Solimões basin. A strong positive gravity anomaly coincides with the axis of the basin, suggesting that shallow ultrabasic bodies were emplaced beneath the rift basins (Milani and Thomaz Filho, 2000). Ultramafic magmatism in rifted areas results from melting of the mantle through decompression, due either to tectonic extension or upwelling of a mantle plume. This suggests that the rifting episode that separated the Guapore and Guyana shields resulted in the formation of a relatively narrow domain in which the high velocity anomaly attributed to the cratonic lithosphere of the Guapore and Guyana shields was significantly attenuated (similar to the model of rift initiation by lithospheric rupture developed by Nicolas et al., 1994).

An interesting feature of our tomographic model of the South American continent is that the southern Paraná basin is characterized by a low velocity anomaly from 200 to at least 375 km depth, overlain by a fast velocity anomaly (Fig. 11). The Paraná basin is

associated with a huge amount of basalts (800,000 km^3), a low eruption rate, and a low stretching factor suggesting that this LIP developed on a thick lithosphere (Turner et al., 1996). The upwelling of the magmatic material probably occurred within a dyke swarm, whose dimensions would not allow it to be imaged in either regional or global tomography. The complex velocity structure might suggest the presence of an abnormally hot mantle, a deep mantle plume, beneath a cratonic lithosphere. In a local P- and S-wave teleseismic tomography of the northern Paraná basin, VanDecar et al. (1995) and Schimmel et al. (2003) found a vertical low velocity anomaly between 200 and 500–600 km depth, with a diameter of about 200 km, located 800 km north of the S-wave low velocity structure shown in our model. The fact that we do not retrieve an S-wave low velocity structure at the same location as VanDecar et al. (1995) and Schimmel et al. (2003) is likely to result from a lack of horizontal resolution that does not allow us to resolve a 200 km narrow structure with long period surface waves. The observation of a low velocity anomaly in the southern part of the Paraná basin suggests that the Paraná LIP might have been related to the upwelling of several plumes. However, the reason why the trace of one or two mantle plume(s), linked to the opening of the south Atlantic Ocean, are still visible under the Paraná basin still remains unclear.

8. Conclusion

We have presented a new and improved shear wave tomographic model of the South American continent which benefits from the use of a large number of surface waveforms including higher modes, providing a dense azimuthal and ray coverage of the South American continent and neighboring oceans. This allows us to discuss new features that have not been observed in previous tomographic models and to confirm some previous results obtained from local and global studies. First we confirm that the seismic signature of the mid oceanic ridges and cratons is rather shallow and does not exceed 150 km for the ridges and 200–250 km for the cratons. In addition to well known large scale heterogeneities, some smaller scale heterogeneities are found, in particular the low velocity signature of the hotspots at the bottom of the oceanic lithosphere. This confirms that structures with horizontal wavelengths smaller than 1000 km can be resolved. The subduction of the Nazca plate beneath the South American continent is associated with a narrow, elongated, high velocity anomaly continuous between 5°S and 37°S at depths from 150 to 250 km. Above 150 km depth, the slab is associated with a succession of low and high velocity anomalies linked to the variation in subduction dip of the Nazca plate. Our model confirms the existence between 15°S and 22°S of a low-velocity anomaly shallower than 150 km depth that probably corresponds to a region in which the mantle wedge and the Andean lower crust underwent partial melting due to fluids released from the subducting plate. Low velocity anomalies are observed at the intersection between the South American margin and the Carnegie and Chile ridges. These low velocity anomalies are related to the shallow hot asthenospheric mantle entrained below the ridge. This explains that the high velocity anomaly associated to the slab progressively vanishes approaching the subducted ridges. In addition, the low velocity anomalies below the continental margin might represent “slab windows” developed through unzipping of the subducted ridges, allowing a transfer of asthenospheric mantle from the shrinking Pacific ocean to the expanding Atlantic ocean.

The model shows an elongated domain of moderately high velocities located beneath the Amazon and Solimões basins and extending down to 100 km depth. This domain separates the Amazonian craton into two high velocity sub-domains corresponding to the northern Guyana and southern Guapore shields, suggesting that the rifting episode responsible for the formation of the Amazon basin has involved a significant part of the lithosphere.

The Paraná basin is underlain by high velocities down to 200 km depth which may correspond to cratonic lithosphere. At greater depth, a low velocity anomaly is located beneath the Ponta Grossa arc at the southern tip of the Paraná basin. This anomaly is located 800 km southward of a narrow S-wave low velocity structure observed in body wave tomography in the depth interval 200 to 500–600 km depth (Schimmel et al., 2003; VanDecar et al., 1995), but irresolvable with long period surface waves. Both anomalies may be related to the Tristan da Cunha plume. Surface and body waves tomographies there-

fore point to a model in which several, most likely diachronous plumes have hit the base of the cratonic lithosphere beneath the Paraná basin. Flood basalts resulting from the melting of the hot plume material probably reached the surface through a system of dike swarms that did not significantly modify the overall seismic properties of the Paraná cratonic lithosphere.

Acknowledgements

We acknowledge financial support from the "Institut National des Sciences de l'Univers" (CNRS-France) through the Programme International de Coopération Scientifique (PICS no. 763). Supercomputer facilities were provided by the "Institut du Développement et des Ressources en Informatique Scientifique" (IDRIS-France). The maps and cross-sections presented in this paper have been produced using the GMT software. We are grateful to Sylvana Pilidou (Cambridge University) for the program allowing to calculate the ray density distribution, Marcelo Assumpção for data from the BLSP experiment and Martin Schimmel for data, a preliminary version of the Paraná tomographic model and fruitful discussions. M. Heintz would like to thank Brian Kennett for a careful reading of the manuscript. The comments from two anonymous reviewers greatly helped improving the manuscript.

References

Allmendinger, R.W., Jordan, T.E., Kay, S.M., Isacks, B.L., 1997. The evolution of the Altiplano-Puna plateau of the central Andes. Annual Review of Earth and Planetary Sciences 25, 139–174.

Barazangi, M., Isacks, B.L., 1979. Subduction of the Nazca plate beneath Peru: evidence from spatial distribution of earthquakes. Geophysical Journal of the Royal Astronomical Society 57, 537–555.

Beck, S., Zandt, G., Myers, S.C., Wallace, T.C., Silver, P.G., Drake, L., 1996. Crustal thickness variations in the central Andes. Geology 24 (5), 407–410.

Cahill, T., Isacks, B.L., 1992. Seismicity and shape of the subducted Nazca plate. Journal of Geophysical Research 97, 17503–17529.

Cara, M., Lévêque, J.J., 1987. Waveform inversion using secondary observables. Geophysical Research Letters 14, 1046–1049.

Cordani, U.G., Brito Neves, B.B., 1982. The geologic evolution of South America during the Archean and early Proterozoic. Revista Brasileira de Geociencias 12 (1–3), 78–88.

Cordani, U.G., Sato, K., Teixeira, W., Tassinari, C.C.G., Basei, M.A.S., 2000. Crustal evolution of the South American platform. In: Cordani, U.G., Milani, E.J., Thomaz-Filho, A. (Eds.), Tectonic Evolution of South America. Folo Producão Editorial. Grafica e Programacão Visual, Rio de Janeiro, pp. 19–40.

Davaille, A., Lees, J.M., 2004. Thermal modelling of subducted plates: tear and hotspot at the Kamchatka corner. Earth and Planetary Science Letters 226, 293–304.

Debayle, E., 1999. SV-wave azimuthal anisotropy in the Australian upper mantle: preliminary results from automated Rayleigh waveform inversion. Geophysical Journal International 137 (3), 747–754.

Debayle, E., Kennett, B.L.N., 2000a. Anisotropy in the Australasian upper mantle from love and rayleigh waveform inversion. Earth and Planetary Science Letters 184, 339–351.

Debayle, E., Kennett, B.L.N., 2000b. The Australian continental upper mantle: structure and deformation inferred from surface waves. Journal of Geophysical Research 105 (11), 25423–25450.

Debayle, E., Kennett, B.L.N., 2003. Surface wave studies of the Australian region. In: Müller, D.H.R. (Ed.), The Evolution and Dynamics of the Australian Plate. Geological Societies of Australia and America.

Debayle, E., Lévêque, J.J., 1997. Upper mantle heterogeneities in the Indian Ocean from waveform inversion. Geophysical Research Letters 24 (3), 245–248.

Debayle, E., Sambridge, M., 2004. Inversion of massive surface wave data sets: model construction and resolution assessment. Journal of Geophysical Research 109 (B2).

Debayle, E., Lévêque, J.J., Cara, M., 2001. Seismic evidence for a deeply rooted low-velocity anomaly in the upper mantle beneath the northeastern Afro/Arabian continent. Earth and Planetary Science Letters 193 (3–4), 423–436.

Debayle, E., Kennett, B.L.N., Priestley, K., 2005. Global azimuthal seismic anisotropy and the unique plate motion deformation of Australia. Nature 433. doi:10.1038/nature03247.

Dickinson, W.R., Snyder, W.S., 1979. Geometry of subducted slabs related to San Andreas transform. Journal of Geology 87 (6), 609–627.

Dorbath, C., Masson, F., 2000. Composition of the crust and uppermantle in the Central Andes (19°30′S) inferred from P velocity and Poisson's ratio. Tectonophysics 327, 213–223.

Dziewonski, M., Anderson, L., 1981. Preliminary reference earth model. Physics of the Earth and Planetary Interiors 25, 297–356.

Engdahl, E.R., Van der Hilst, R.D., Berrocal, J., 1995. Imaging of subducted lithosphere beneath South America. Geophysical Research Letters 22 (16), 2317–2320.

Engdahl, E.R., Van der Hilst, R.D., Buland, R., 1998. Global teleseismic earthquake relocation with improved travel times and procedures for depth determination. Bulletin of the Seismological Society of America 88, 722–743.

Gansser, A., 1973. Facts and theories on the Andes. Journal of the Geological Society (London) 129, 93–131.

Grand, S.P., 1994. Mantle shear structure beneath the Americas and surrounding oceans. Journal of Geophysical Research 99 (B6), 11591–11621.

Haberland, C., Rietbrock, A., 2001. Attenuation tomography in the western central Andes: a detailed insight into the structure of a magmatic arc. Journal of Geophysical Research 106 (B6), 11151–11167.

Hamza, V.M., Muñoz, M., 1996. Heat flow map of South America. Geothermics 25 (6), 599–646.

Helffrich, G., Wiens, D.A., Vera, E., Barrientos, S., Shore, P., Robertson, S., Adaros, R., 2002. A teleseismic shear-wave splitting study to investigate mantle flow around South America and implications for plate-driving forces. Geophysical Journal International 149, F1–F7.

James, D.E., Snoke, J.A., 1990. Seismic evidence for continuity of the deep slab beneath central and eastern Peru. Journal of Geophysical Research 95 (B4), 4989–5001.

James, D.E., Assumpção, M., Snoke, J.A., Ribotta, L.C., Kuehnel, R., 1993. Seismic studies of continental lithosphere beneath SE Brazil. Anais da Academia Brasileira de Ciencias 65 (Suppl. 2), 227–250.

Johnston, S.T., Thorkelson, D.J., 1997. Cocos-Nazca slab window beneath Central America. Earth and Planetary Science Letters 146, 465–474.

Kennett, B.L.N., 1995. Approximations for surface-wave propagation in laterally varying media. Geophysical Journal International 122, 470–478.

King, S.D., Ritsema, J., 2000. African hotspot volcanism: small-scale convection in the upper mantle beneath cratons. Science 290, 1137–1140.

Krüger, F., Scherbaum, F., Rosa, J.W.C., Kind, R., Zetsche, F., Höhne, J., 2002. Crustal and upper mantle structure in the Amazon region (Brazil) determined with broadband mobile stations. Journal of Geophysical Research 107 (10), ESE 17-1–ESE 17-12.

Lagabrielle, Y., Guivel, C., Maury, R.C., Bourgois, J., Fourcade, S., 2000. Magmatic-tectonic effects of high thermal regime at the site of active ridge subduction: the Chile triple junction model. Tectonophysics 326, 255–268.

Lesquer, A., De Almeida, F.F.M., Davino, A., Lachaud, J.C., Maillard, P., 1981. Signification structurale des anomalies gravimétriques de la partie sud du craton de São Francisco (Brésil). Tectonophysics 76, 273–293.

Levin, V., Shapiro, N., Park, J., Ritzwoller, M., 2002. Seismic evidence for catastrophic slab loss beneath Kamchatka. Nature 418 (6899), 763–767.

Levin, V., Shapiro, N., Park, J., Ritzwoller, M., in press. The slab portal beneath the western Aleutians, Geology.

Martin, H., 1999. Adakitic magmas: modern analogues of Archean granitoids. Lithos 46, 411–429.

Masson, F., Dorbath, C., Martinez, C., Carlier, G., 2000. Local earthquake tomography of the Andes at 20°S: implications for the structure and building of the moutain range. Journal of South American Earth Sciences 13, 3–19.

Mégnin, C., Romanowicz, B., 2000. The shear velocity structureof the mantle from the inversion of body, surface and higher modes waveforms. Geophysical Journal International, 143709–143728.

Milani, E.J., Thomaz Filho, A., 2000. Sedimentary basins of South America. In: Cordani, U.G. (Ed.), Tectonic Evolution of South America, Rio de Janeiro, p. 856.

Montagner, J.P., 1986. Regional three-dimensional structures using long-period surface waves. Annales Geophysicae, B (3), 283–294.

Montelli, R., Nolet, G., Dahlen, F.A., Masters, G., Engdahl, E.R., Hung, S.H., 2004. Finite-frequency tomography reveals a variety of plumes in the mantle. Science 303, 338–343.

Myers, S.C., Beck, S., Zandt, G., Wallace, T., 1998. Lithospheric-scale structure across the Bolivian Andes from tomographic images of velocity and attenuation for P and S waves. Journal of Geophysical Research 103 (B9), 21233–21252.

Nataf, H.C., Ricard, Y., 1996. 3SMAC : an a-priori tomographic model of the upper mantle based on geophysical modelling. Physics of the Earth and Planetary Interiors 95, 101–122.

Nicolas, A., Achauer, U., Daignières, M., 1994. Rift initiation by lithospheric rupture. Earth and Planetary Science Letters 123 (281-298).

Nishimura, C.E., Forsyth, D.W., 1989. The anisotropic structure of the upper mantle in the Pacific. Geophysical Journal of the Royal Astronomical Society 96 (2), 203–229.

Parmentier, E.M., Turcotte, D.L., Torrance, K.E., 1975. Numerical experiments on the structure of mantle plumes. Journal of Geophysical Research 80 (32), 4417–4424.

Pilidou, S., Priestley, K., Gudmundsson, O., Debayle, E., 2004. Upper mantle S-wave speed heterogeneity beneath the north Atlantic and surrounding region from regional surface wave tomography: the Iceland and Azores plumes. Geophysical Journal International 159, 1057–1076.

Priestley, K., Debayle, E., 2003. Seismic evidence for a moderately thick lithosphere beneath the Siberian platform. Geophysical Research Letters 30 (3), 1118.

Ramos, V.A., Aleman, A., 2000. Tectonic evolution of the Andes. In: Cordani, U.G. (Ed.), Tectonc Evolution of South America, Rio de Janeiro, p. 856.

Ritsema, J., van Heijst, H.J., Woodhouse, J.H., 1999. Complex shear wave velocity structure imaged beneath Africa and Iceland. Science 286, 1925–1928.

Ritsema, J., van Heijst, H.J., Woodhouse, J.H., 2004. Global transition zone tomography. Journal of Geophysical Research 109 (B2).

Russo, R.M., Silver, P.G., 1994. Trench-Parallel flow beneath the Nazca plate from seismic anisotropy. Science 263, 1105–1111.

Schimmel, M., Assumpção, M., VanDecar, J.C., 2003. Seismic velocity anomalies beneath SE Brazil from P and S wave travel time inversions. Journal of Geophysical Research 108 (B4). doi:10.1029/2001JB000187.

Schneider, J.F., Sacks, I.S., 1987. Stress in the contorted Nazca plate beneath southern Peru from local earthquakes. Journal of Geophysical Research 92 (13), 13887–13902.

Schurr, B., 2001. Seismic Structure of the Central Andean Subduction Zone from Local Earthquake Data. GeoForschungsZentrum Potsdam, Potsdam. 123 pp.

Sieminski, A., Debayle, E., Lévêque, J.J., 2003. Seismic evidence for deep low-velocity anomalies in the transition zone beneath West Antarctica? Earth and Planetary Science Letters 216 (4), 645–661.

Silveira, G., Stutzmann, E., 2002. Anisotropic tomography of the Atlantic Ocean. Physics of the Earth and Planetary Interiors 132, 237–248.

Silveira, G., Stutzmann, E., Griot, D.A., Montagner, J.P., Victor, L.M., 1998. Anisotropic tomography of the Atlantic ocean from Rayleigh surface waves. Physics of the Earth and Planetary Interiors 106, 257–273.

Smith, G.P., Wiens, D.A., Fischer, K.M., Dorman, L.M., Webb, S.C., Hildebrand, J.A., 2001. A complex pattern of mantle flow in the Lau backarc. Science 292, 713–716.

Snoke, J.A., James, D.E., 1997. Lithospheric structure of the chaco and paraná basins of South America from surface-wave inversion. Journal of Geophysical Research 102 (B2), 2939–2951.

Swenson, J.L., Beck, S.L., Zandt, G., 2000. Crustal structure of the altiplano from broadband regional waveform modelling: implications for the composition of thick continental crust. Journal of Geophysical Research 105 (B1), 607–621.

Tarantola, A., Valette, B., 1982. Generalized nonlinear inverse problems solved using the least squares criterion. Reviews of Geophysics and Space Physics 20 (2), 219–232.

Tassinari, C.C.G., Macambira, M.J.B., 1999. Geochronological provinces of the Amazonian craton. Episodes 22 (3), 174–182.

Tassinari, C.C.G., Bettencourt, J.S., Geraldes, M.C., Macambira, M.J.B., Lafon, J.M., 2000. The Amazonian craton. In: Cordani, U.G. (Ed.), Tectonic Evolution of South America, Rio de Janeiro, p. 856.

Teixeira, W., Sabaté, P., Barbosa, J., Noce, C.M., Carneiro, M.A., 2000. Archean and Paleoproterozoic tectonic evolution of the São Francisco craton, Brazil. In: Cordani, U.G. (Ed.), Tectonic Evolution of South America, Rio de Janeiro, p. 856.

Trampert, J., Woodhouse, J.H., 1995. Global phase velocity maps of love and Rayleigh waves between 40 and 150 seconds. Geophysical Journal International 122 (2), 675–690.

Turner, S., Regelous, M., Kelley, S., Hawkesworth, C., Mantovani, M., 1994. Magmatism and continental break-up in the South Atlantic: high precision ^{40}Ar–^{39}Ar geochronology. Earth and Planetary Science Letters 121, 333–348.

Turner, S., Hawkesworth, C., Gallagher, K., Stewart, K., Peate, D., Mantovani, M., 1996. Mantle plumes, flood basalts, and thermal models for melt generation beneath continents: assessment of a conductive heating model and application to the Paraná. Journal of Geophysical Research 101 (B5), 11503–11518.

VanDecar, J.C., James, D.E., Assumpção, M., 1995. Seismic evidence for a fossil mantle plume beneath South America and implications for plate driving forces. Nature 378, 25–31.

Van der Lee, S., James, D.E., Silver, P.G., 2001. Upper mantle S velocity structure of central and western South America. Journal of Geophysical Research 106, 1–14.

Van der Lee, S., James, D.E., Silver, P.G., 2002. Correction to "Upper mantle S-velocity structure of western and central South America". Journal of Geophysical Research 107. doi:10.1029/2002JB001891.

Vdovin, O., Rial, J.A., Levshin, A.L., Ritzwoller, M.H., 1999. Group-velocity tomography of South America and the surrounding oceans. Geophysical Journal International 136, 324–340.

Wallace, T.C., Zandt, G., Jiao, W., 1997. Modelling the near-and intermediate-terms of the displacement field from deep earthquakes. Eos Transactions, AGU 78 (46), 449.

Wortel, M.J.R., 1984. Spatial and temporal variations in the Andean subduction zone. Journal of the Geological Society (London) 141 (5), 783–791.